

# Factors affecting suspended-solids concentrations in South San Francisco Bay, California

David H. Schoellhamer

U.S. Geological Survey, Sacramento, California

**Abstract.** Measurements of suspended-solids concentration (**SSC**) were made at two depths at three sites in South San Francisco Bay (**South Bay**) to determine the factors that affect **SSC**. Twenty-eight segments of reliable and continuous **SSC** time series data longer than 14 days were collected from late 1991 or 1992 through September 1993. Spectral analysis and singular spectrum analysis were used to relate these data segments to time series of several potential forcing factors, including diurnal and semidiurnal tides, the spring-neap tidal cycle, wind shear, freshwater runoff, and longitudinal density differences. **SSC** is greatest during summer when a landward wind shear is applied to South Bay by the afternoon sea breeze. About one half the variance of **SSC** is caused by the spring-neap cycle, and **SSC** lags the spring-neap cycle by about 2 days. Relatively short duration of slack water limits the duration of deposition of suspended solids and consolidation of newly deposited bed sediment during the tidal cycle, so suspended solids accumulate in the water column as a spring tide is approached and slowly deposit as a neap tide is approached. Perturbations in **SSC** caused by wind and local runoff from winter storms during the study period were usually much smaller than **SSC** variations caused by the spring-neap cycle. Variations of **SSC** at the study sites at tidal timescales are tidally forced, and nonlinear physical processes are significant. Advective transport dominates during spring tides when water with higher **SSC** due to wind wave resuspension is advected to the main channel from shallow water, but during neap tides, advective transport is less significant. The findings of this and other studies indicate that the tidally averaged transport of suspended solids responds to seasonal variations of wind shear in South Bay.

## Introduction

The supply and fate of trace metals in South Bay, which are dependent upon the particulate matter in the estuary, are important management issues for South San Francisco Bay (Figure 1). South Bay receives many wastewater discharges, primarily south of the Dumbarton Bridge, that contain trace metals that accumulate in benthic organisms [Luoma *et al.*, 1985]. Trace metals tend to adsorb to particulate matter [Kuwabara *et al.*, 1989], so the fate of trace metals is partly determined by the fate of suspended solids. Concentrations of dissolved metals are greater in South Bay than elsewhere in San Francisco Bay, and bottom sediments are believed to be a significant source [Flegal *et al.*, 1991].

Suspended and benthic particulate matter affect the habitat and water chemistry of South Bay in several other ways. Particulate matter provides the habitat for benthic communities, and seasonal changes in sediment erosion and deposition patterns contribute to seasonal changes in abundance of benthic macroinvertebrates [Nichols and Thompson, 1985]. Tidal marshes are an ecologically important habitat along the margins of South Bay that were created and are maintained by sedimentation processes [Arwater *et al.*, 1979]. The sediments and pore water at the bottom of South Bay are a reservoir of nutrients, metals, and other substances in which chemical reactions occur and which provide an important source and/or sink to the water column [Hammond *et al.*, 1985; Flegal *et al.*, 1991]. Suspended solids confine the photic zone to the upper part of the water column, and this limitation on light

availability is a major control on phytoplankton production in San Francisco Bay [Cloern, 1987].

Particulate matter in the benthos and in suspension is an important component of the South Bay Estuary. The purpose of this paper is to determine the factors affecting suspended-solids concentrations in South San Francisco Bay by analyzing time series of suspended-solids concentrations (SSCs).

## Study Area

The hydrodynamics of South San Francisco Bay are controlled by tides, winds, and freshwater runoff. The tides form standing waves in South Bay, and the tidal amplitudes increase in the landward (southeasterly) direction. During a tidal cycle the maximum seaward excursion occurs at low tide, and the maximum landward excursion occurs at high tide because of the standing wave. Spring tidal currents are typically about  $100 \text{ cm s}^{-1}$  in a deep (about 14 m mean lower low water (MLLW)) channel along the axis of South Bay and about  $40 \text{ cm s}^{-1}$  in shallow water (about 2 m MLLW) adjacent to the channel [Cheng and Gartner, 1985]. Tides also have a fortnightly spring-neap variability. Tidally driven, residual circulation is extremely weak south of the San Mateo Bridge [Walters *et al.*, 1985].

During the spring and summer an afternoon northwesterly sea breeze is present [Gilliam, 1962]. Northwesterly winds establish a wind-driven circulation pattern in the bay south of the San Mateo Bridge, with a landward flow in shallow water and a seaward return flow in the main channel [Conomos and Peterson, 1977; Cheng and Gartner, 1985; Walters *et al.*, 1985; Lacy *et al.*, 1996].

Winter runoff from the Sacramento-San Joaquin Delta and local sources can affect hydrodynamics in South Bay [Walters *et*

This paper is not subject to U.S. copyright. Published in 1996 by the American Geophysical Union.

Paper number 96JC00747.

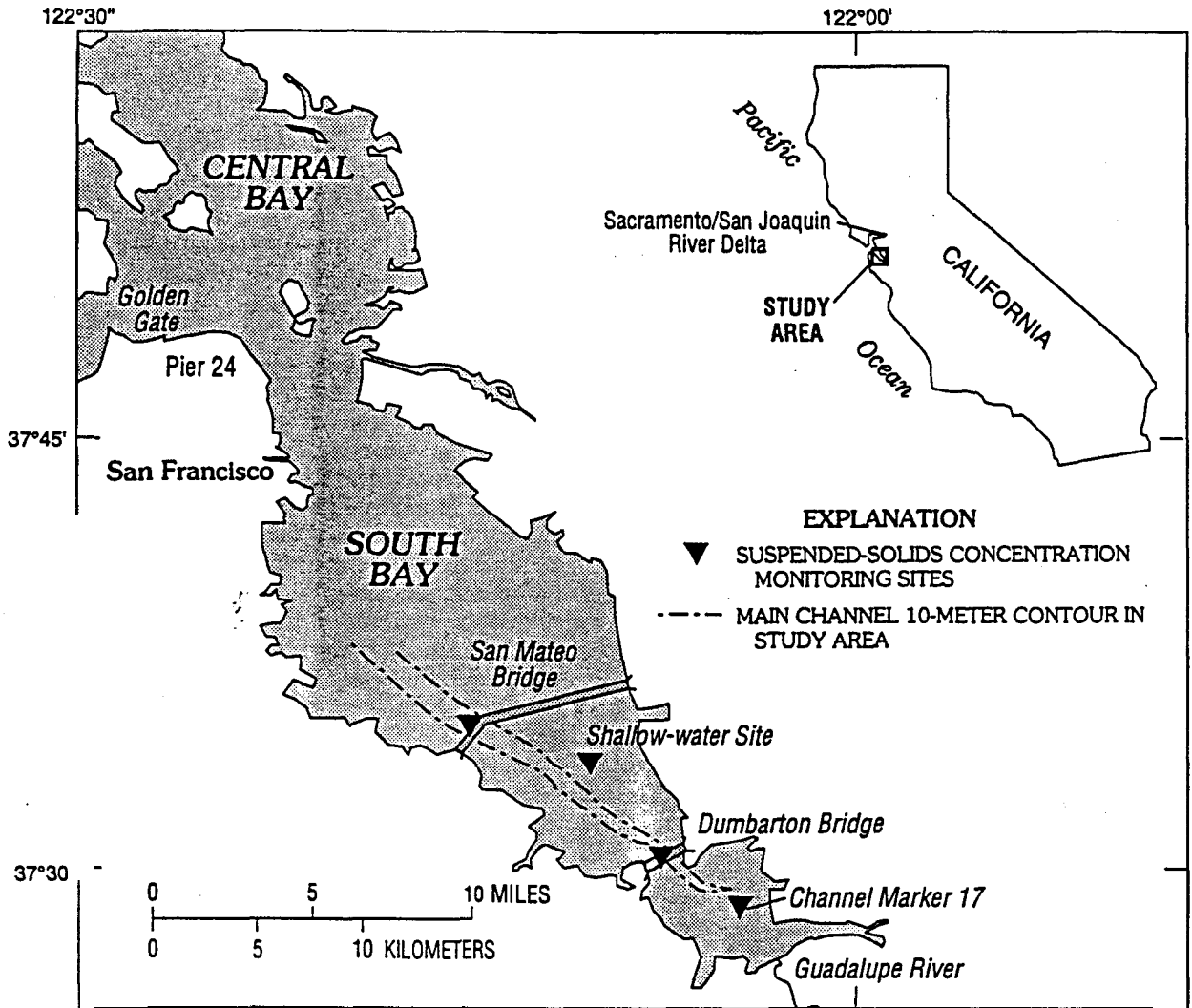


Figure 1. South San Francisco Bay study area.

*al.*, 1985]. Precipitation occurs primarily during winter, and the resulting winter and spring freshwater runoff from the Delta makes salinities in Central Bay smaller than salinities in South Bay. **Baroclinic** circulation with a seaward bottom flow in the main channel can occur. As Delta runoff subsides, salinities in Central Bay can **increase** as oceanic waters return through the Golden Gate and become greater than in South Bay, and the **baroclinic** circulation can reverse. During very wet winters, freshwater inflow at the extreme south end of the bay can significantly affect hydrodynamics in South Bay.

Bottom sediments in South Bay are composed primarily of silts and clays [Folger, 1972; Thompson *et al.*, 1981]. Sediments from the Delta account for 86% of the fluvial sediment supply to San Francisco Bay [Porterfield, 1980]. Plumes of suspended sediment from the Delta have been observed to extend into South Bay north of the San Mateo Bridge [Carlson and McCulloch, 1974; Powell *et al.*, 1989]. Powell *et al.* [1989] conducted four cruises in South Bay in spring 1987 and observed that SSCs were greater during spring tides than during neap tides and that wind wave resuspension in shallow water increased SSC. **Time series** of tidal velocity, wave properties, and SSC at a shallow-water site in South Bay [Buchanan *et al.*, 1996, Figure 1] indicate that wind waves resuspend bottom sediments and that northwesterly winds generate a southeasterly flux of suspended solids [Lacy *et al.*, 1996].

## Methods

Data collection and analysis methods were selected to permit analysis of SSC time series from tidal to seasonal timescales. **Time series** of potential forcing factors were compiled, analyzed, and compared with SSC time series.

## Data Collection

Optical backscatterance (OBS) sensors were used to measure SSC in South Bay [Buchanan and Schoellhamer, 1995]. OBS sensors emit a pulse of infrared light, some of which scatters off suspended particles, returns to the sensor, and is measured [Downing *et al.*, 1981]. Sensors were deployed at the following three sites in the main channel: the San Mateo Bridge, the Dumbarton Bridge, and channel marker 17 (Figure 1). **Two sensors** were deployed at each site, one at **middepth** and another at 1 to 2 m above the bottom. Measurements were taken every 15 min. In addition, time series of velocity, depth, wave properties, and SSC were collected at a shallow-water site (2.1 m MLLW, Figure 1) in March 1994 [Buchanan *et al.*, 1996].

Servicing trips were conducted every 1 to 5 weeks to clean the channel OBS sensors and to collect water samples for sensor calibration. OBS sensors in shallow estuarine environments are susceptible to fouling [Schoellhamer, 1993], and fouling limited the

length of reliable and continuous segments of data available from each sensor to about 2 to 70 days. Field calibrations of the OBS sensors were developed by comparing sensor output to the SSC of water samples [Fisch and Friedman, 1989]. The standard errors of the OBS sensor calibrations are given in Table 1. If more than one OBS sensor was used at a site, then the mean error, weighted by the duration of the sensor deployment, is given.

### Data Analysis

Channel data collected from the time of deployment (Table 1) through September 30, 1993, were considered in the analysis, and the longest segments of nearly continuous data at each site were identified. The criteria used to identify the data segments were (1) time period greater than 14 days and (2) no gaps greater than 3 hours. A minimum length of 14 days was required to allow identification of the fortnightly spring-neap cycle, and gaps were filled with linear interpolation. A total of 28 data segments 14 to 70 days long were identified, and the time series were decimated to an hourly time step.

Time series of several potential hydrodynamic and meteorological forcing mechanisms were developed for comparison to SSC time series. Water level and velocity at the Dumbarton Bridge were calculated from tidal harmonic constants determined from water-level measurements [Cheng and Gartner, 1984, 1985]. The strength of the spring-neap cycle was quantified by calculating the low-pass root-mean-square (RMS) water level  $h_{rms}$  by squaring the calculated water level, low-pass filtering, and taking the square root. All low-pass filtering was performed with an 11th order Butterworth filter with a cutoff frequency of 0.0271 hour<sup>-1</sup>. Gaged discharge Q from the Guadalupe River was used as an indicator of local runoff [Palmer et al., 1994]. Measured salinity and water temperature at the San Mateo Bridge and San Francisco Pier 24 were used to determine the density difference  $\Delta\rho$  between South and Central Bays. Northerly, easterly, and landward (135° clockwise from north) components of wind-shear stress ( $\tau_n$ ,  $\tau_e$ , and  $\tau_l$ ) were estimated from wind data collected at San Francisco Airport, and drag coefficients were from Garratt [1977]. Wind velocity varies horizontally in South Bay, so these estimated wind-shear stress components are only an approximation of the true stresses. Barometric pressure  $p_a$  at San Francisco Airport also was considered in the analysis.

Three approaches were used to determine the factors affecting SSC in South San Francisco Bay. First, the mean concentrations of the 28 lengthy data segments were nondimensionalized (divided by) by the mean site concentrations (Table 1) and compared to concurrent mean values of the hydrodynamic and meteorological forcing to identify seasonal trends and correlations.

Ideally, continuous time series collected at all of the study sites for at least a year would have been used to determine seasonal trends. Instrument fouling limited the length of the available time series, however, so intercomparison of the data segments and forcing was used instead.

Second, spectral analysis was used to determine the most energetic frequency bands in the SSC and forcing time series. The minimum SSC segment length was 336 hours, and a 256-point fast Fourier transform with a Hanning window was used for the spectral analysis. Thus the spectral analysis is limited to frequencies greater than 1/36 hour<sup>-1</sup>.

Third, intrasegment analysis was performed with singular spectrum analysis [Vautard et al., 1992]. Singular spectrum analysis (SSA) is essentially a principal components analysis in the time domain that extracts information from short and noisy time series without prior knowledge of the dynamics affecting the time series [Vautard et al., 1992; Derringer et al., 1995]. For a standardized time series  $x_i$ , where sample index  $i$  varies from 1 to  $N$ , a lagged autocorrelation matrix is formed with maximum lag (or window size)  $M$ . The eigenvalues  $\lambda_k$  and eigenvectors (or empirical orthogonal functions)  $E_j^k$  of this matrix are determined and sorted in descending order of  $\lambda_k$ , where indices  $j$  and  $k$  vary from 1 to  $M$ . The  $k$ th principal component is

$$a_i^k = \sum_{j=1}^M x_i + j E_j^k, \quad 0 \leq i \leq N-M \quad (1)$$

Each component of the original time series identified by SSA can be reconstructed, with the  $k$ th reconstructed component (RC) series given by

$$x_i^k = \frac{1}{M} \sum_{j=1}^M a_{i-j}^k E_j^k, \quad M \leq i \leq N-M+1. \quad (2)$$

Expressions for  $x_i^k$  for  $i < M$  and  $i > N-M+1$  are given by Vautard et al. [1992]. The fraction of the total variance of the original time series (equal to 1 for standardized time series) contained in the  $k$ th RC is  $\lambda_k$ , so that with the sorting used the RCs are ordered by decreasing information about the original time series. Most of the variance is contained in the first several RCs, and most or all of the remaining RCs contain noise. SSA typically decomposes a time series into RCs that are nearly periodic, with one or two dominant periods. One or two RCs contain variations in the time series with periodicities greater than  $M$ . A pair of RCs with similar  $\lambda_k$  normally represents each period less than  $M$  with significant energy in the original time series. In this paper, SSA is used to determine the most significant RCs of the 28 SSC time series, and these RCs are compared with the RCs of selected forcing mechanisms. A window size  $M$  of 30 hours was used to separate tidal and subtidal signals.

## Results

Results will be presented in the following three sections: (1) intersegment comparison of SSC and forcing factors, (2) spectral analysis of SSC and forcing factors, and (3) intrasegment comparison of RCs and forcing factors.

### Intersegment Comparison of SSC and Forcing Factors

Nondimensionalized mean segment concentrations were compared with the concurrent mean values of the potential forcing

Table 1. Summary of South Bay Suspended-Solids Concentrations

Site	Deployment Date	Sensor Elevation	Standard Error of OBS Sensor(s), mg L <sup>-1</sup>	Mean SSC, mg L <sup>-1</sup>
San Mateo Bridge	Dec. 23, 1991	middepth	10.7	65.7
		near bottom	14.1	95.2
Dumbarton Bridge	Oct. 22, 1992	middepth	14.5	12.9
		near bottom	20.4	95.6
Channel marker 17	Feb. 26, 1992	middepth	17.6	121
		near bottom	14.2	170

OBS is optical backscatterance.

Table 2. Correlation Coefficients of Mean Forcing Factors and Mean Segment Concentrations

Forcing Factors	Definition	r
$h_{\text{rms}}$	root-mean-square water level	0.289
$Q$	gaged discharge of <b>Guadalupe</b> River	-0.383
$\Delta\rho$	density difference between South and <b>Central</b> Bays	0.396
$\tau_l$	landward component of wind-shear stress	0.661
$\tau_n$	northerly component of wind-shear stress	-0.722
$\tau_e$	easterly component of wind-shear stress	0.602
$P_a$	barometric pressure	-0.112

factors to identify the significant forcing factors on a seasonal timescale. The nondimensionalized mean segment concentration  $C_b$  is defined as the mean segment concentration divided by the mean concentration for the entire period of record (Table 1). Correlation coefficients  $r$  for  $C_b$  and the forcing factors are shown in Table 2.

The greatest  $|r|$  is for the northerly component of the wind-shear stress ( $r = -0.722$ ), and the significance level is less than 0.0001 (Figure 2). SSCs are greatest when the southerly component of wind-shear stress is greatest, which occurs during the spring and summer. The correlation of  $C_b$  with  $\tau_l$ , which is dependent on  $\tau_n$ , is slightly less ( $r = 0.661$ ). The other forcing factors are not as well correlated with  $C_b$ .

Spectral Analysis of SSC and Forcing Factors

The mean spectral density of the 28 SSC data segments indicates that the greatest energy is at subtidal frequencies and at the semidiurnal frequency, and other energy peaks are present at tidal and tidal harmonic frequencies of about  $n/24$ , where integer  $n$  varies from 1 (0.04167 hour<sup>-1</sup>) to 10 (0.4167 hour<sup>-1</sup>) (Figure 3). Spectral density in Figure 3 is nondimensionalized by dividing by the mean spectral density. The magnitude of the diurnal spectral peak is similar for both winter and summer data segments, which indicates that the daily cycle of shallow-water resuspension and deposition caused by the daily sea breeze is not observed at the channel sites.

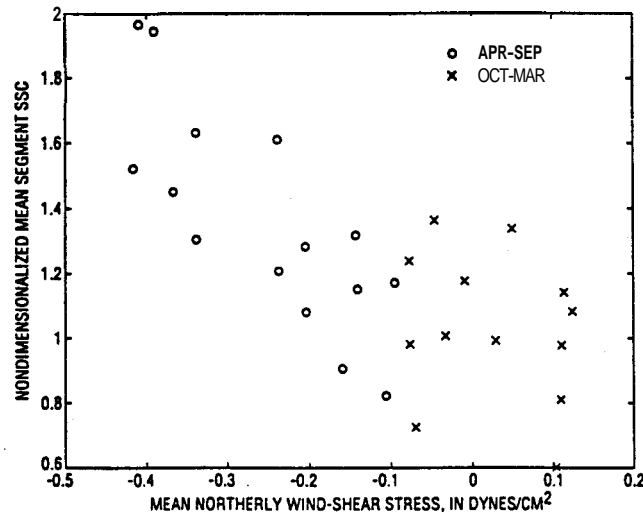


Figure 2. Correlation of northerly wind-shear stress and nondimensionalized mean segment suspended-solids concentration (SSC).

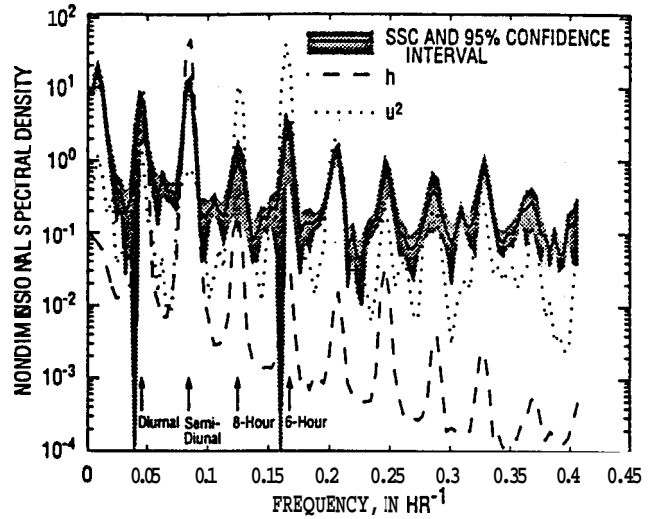


Figure 3. Mean spectral density of SSC from the 28 data segments and spectral density of water level  $h$  and squared velocity  $u^2$  at the Dumbarton Bridge.

Spectra of potential tidal forcing factors are similar to the SSC spectra. One tidal process that may affect SSC is advective transport of suspended solids. Within a tidal cycle the masses of water and suspended solids are at their maximum seaward extent at low tide and at their maximum landward extent at high tide. In South Bay, because of the nearly standing tidal wave, advective transport can be represented by the water-surface elevation  $h$ . Resuspension by tidal currents also can affect SSC, and the shear force of the tidal current on the bed is roughly proportional to the squared velocity  $u^2$ . Spectra of  $h$  and  $u^2$  were determined from data collected at the Dumbarton Bridge [Cheng and Gartner, 1984, 1985] and are presented in Figure 3. These spectra contain peaks at  $n/24$  frequencies and relatively less energy at subtidal frequencies. Most of the energy in the  $h$  spectrum is at the diurnal and semidiurnal frequencies, with relatively little energy at the diurnal-semidiurnal tidal harmonic frequencies ( $n \geq 3$ ). Nonlinear physical processes transfer energy from diurnal and semi-diurnal frequencies to the tidal harmonic frequencies. Squared velocity is a nonlinear term, so the greatest spectral peaks correspond to  $n = 3$  and 4 (6- and 8-hour periods), and the other tidal harmonic peaks are more significant than for  $h$ . The SSC spectrum is more similar to the  $u^2$  spectrum than the  $h$  spectrum because nonlinear physical processes are less significant for  $h$ . Therefore variations of SSC at the study sites at tidal timescales are tidally forced, and nonlinear physical processes are significant.

Singular Spectrum Analysis of Segment SSC

A typical result of SSA is presented in Figure 4 for an SSC data segment from the middepth sensor at the Dumbarton Bridge. The most significant RC (RC1) for this segment is the subtidal variation of SSC, which contains 31.2% of the total SSC variance ( $\lambda_1 = 0.312$ ). RC1 represents the variation in SSC caused by the spring-neap cycle, which will be discussed in the next section. RC2 and RC3 primarily contain the diurnal variation of SSC as determined from their spectra, and their sum is shown in Figure 4 (RC23,  $\lambda_2 + \lambda_3 = 0.241$ ). RC23 also contains some variance caused by the spring-neap cycle. The other RC pairs contain the semidiurnal variation (RC45,  $\lambda_4 + \lambda_5 = 0.150$ ), 6-hour tidal harmonic period (RC67,  $\lambda_6 + \lambda_7 = 0.113$ ), and 8-hour tidal harmonic period (RC89,  $\lambda_8 + \lambda_9 = 0.082$ ). The nine modes shown on Figure 4 contain 89.8% of the SSC variance.

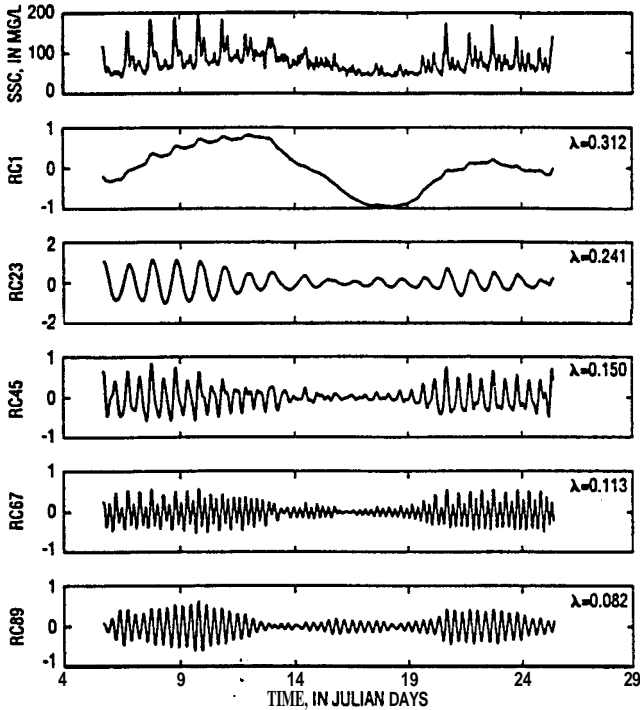


Figure 4. Example singular spectrum analysis (SSA) results for a data segment from middepth at the Dumbarton Bridge, 1993.

Spring-neap cycle. The lagged covariances between the SSA RC that contained the subtidal SSC variations and low-pass filtered forcing factors were calculated for each data segment to determine which forcing factors were most significant between the seasonal and tidal timescales. For every data segment the most significant RC (RC1) contained subtidal SSC variations; no other RCs contained significant subtidal variations. The mean variance contained by RC1 was 50.9%. RC1 was well correlated with the spring-neap cycle, quantified by  $h_{rms}$  ( $r = 0.800$ ) and lagged  $h_{rms}$  by an average of 32.9 hours. Figure 5 presents  $h_{rms}$ , SSC, and RC1 for the same time series from the Dumbarton Bridge shown in Figure 4 for which  $r = 0.883$  when SSC lags behind  $h_{rms}$  by 49 hours. A spring tide at day 8 is followed by a maximum of RC1 at day 12, a neap tide at day 15 is followed by a

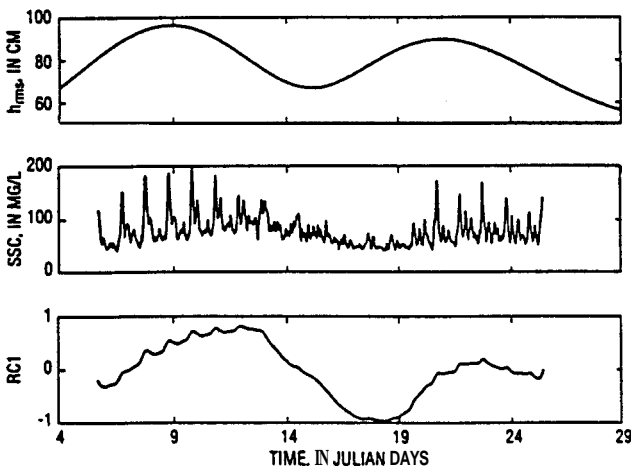


Figure 5. Variation of SSC and RCI with the spring-neap cycle ( $h$ ) for a data segment from middepth at the Dumbarton Bridge, 1993.

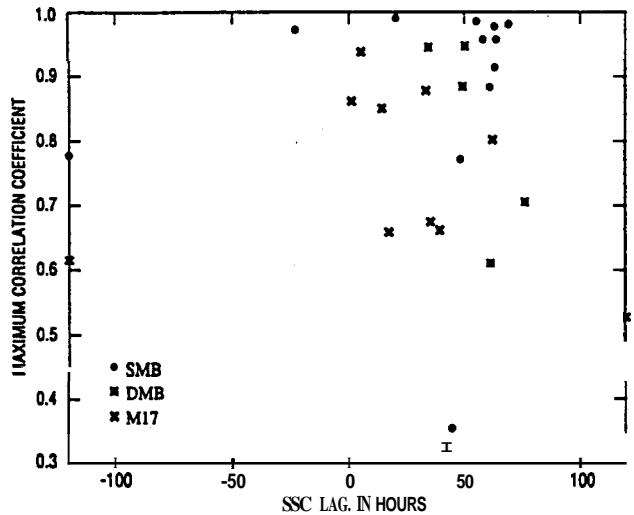


Figure 6. Lagged covariance of  $h_{rms}$  and RC1 for the 28 data segments. SMB is San Maw, Bridge, DMB is Dumbarton Bridge, and M17 is marker 17.

minimum of RC1 at day 18, and a spring tide at day 21 is followed by a maximum of RC1 at day 22. The scatterplot of RC1 lag and  $r$  for the 28 data segments shows that for most data segments the maximum  $r$  is between 0.6 and 1.0 when RC1 lags  $h_{rms}$  by between 0 and 70 hours (Figure 6). Values for five segments are outliers (lag equals  $\pm 120$  hours or  $r < 0.4$  in Figure 6). Four of these outliers were for data segments with small variations in the spring-neap cycle, which occur in late March and late September. The other apparent outlier (marker 17,  $r = 0.325$ ) was for the longest data segment (1665 hours), and the significance level of the correlation was less than 0.0001. Ignoring the five outliers, the mean maximum  $r$  is 0.861, the mean lag of RC1 compared with  $h_{rms}$  is 41.5 hours (Table 3), and the significance levels of the correlations are less than 0.0001.

Other low-frequency forcing factors were not correlated with SSC or RC1. Wind and local runoff from specific winter storms sometimes increased SSC and RC1, but these perturbations were usually much smaller than the spring-neap variation. For the data segment shown in Figures 4 and 5, winter storms occurred during days 13, 20, and 22, and the largest runoff Q during the study period occurred during days 12 through 15, but these storms did not significantly affect SSC at the Dumbarton Bridge. The runoff increased SSC at marker 17 for about 2 days to amounts typical of a spring tide.

Spring-neap cycle and tidal advection. A common tendency of the SSC data is that the maximum concentration in the channel

Table 3. Correlation of RC1 and  $h_{rms}$ , Lag of RC1 from  $h_{rms}$ , and Percent Variance Contained in RC1

Site	Mean Correlation Coefficient	Mean Lag, hours	Mean Percent of Variance Contained in RC1
San Mnteo Bridge	0.939	47.8	62.6
Dumbarton Bridge	0.819	54.0	51.7
Channel marker 17	0.791	25.8	35.5
All	0.861	41.5	50.8

RC1 is the first reconstructed component. Five outliers in Figure 5 are ignored.

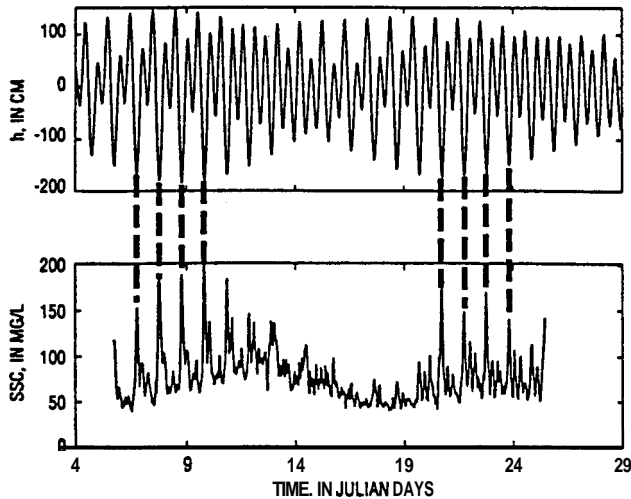


Figure 7. Example of SSC maxima at low spring tides (vertical dashed lines) for a data segment from **middepth** at the Dumbarton Bridge, 1993. SSC is a measured value; h is a calculated value.

occurs at low tide (slack **after** ebb tide due to the standing wave in South Bay), especially during spring tides. Figure 7 shows the water-surface elevation and SSC for the example data set from the Dumbarton Bridge. Another example is data collected on March 15, 1994, from **middepth** at the San Mateo Bridge and at the **shallow-water** site (Figure 8). SSC at the San Mateo Bridge is about  $50 \text{ mg L}^{-1}$ , except during the **midmorning** low (slack after ebb) tidewhen SSC increases to  $120 \text{ mg L}^{-1}$ . The afternoon ebb tide is weaker, and no significant increase in SSC is observed at the bridge. SSC at the shallow-water site is usually about  $120 \text{ mg L}^{-1}$ , except during early morning and afternoon high (slack after flood) tides when SSC decreases to  $50$  to  $60 \text{ mg L}^{-1}$ . Thus the data in Figures 7 and 8 indicate that tides transport suspended solids between the channel and shallow water and that SSC maxima in the channel are probably caused by advection of water with large SSC from shallow water.

To investigate the relation of tidal advection and SSC, the **diurnal and semidiurnal SSA RCs** of h and SSC can be compared. The diurnal and semidiurnal **RCs** are studied because they **repre-**

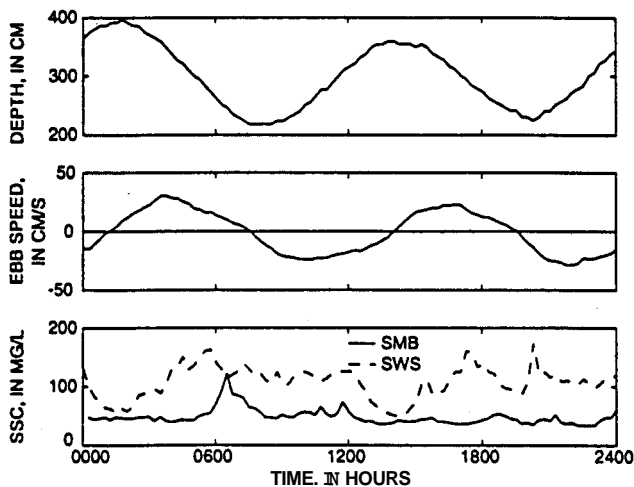


Figure 8. Variation of SSC at **middepth** at the San Mateo Bridge (SMB) and at the **shallow-water** site (SWS) with water depth and ebb current speed at the shallow-water site on March 15, 1994. The direction of ebb tide at the shallow-water site is to the north-west.

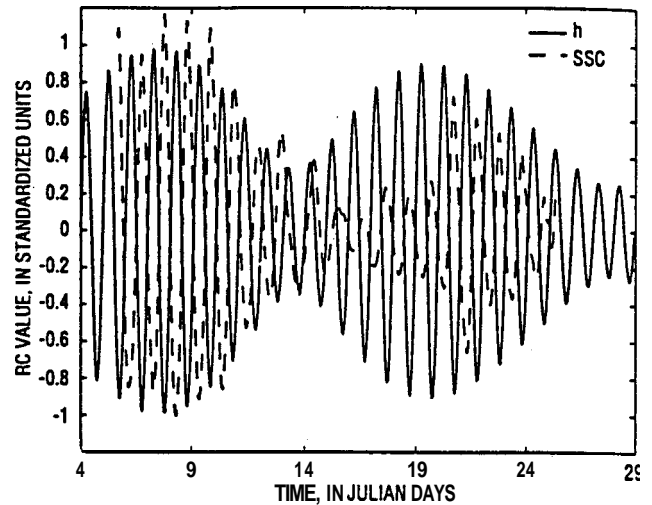


Figure 9. Example of diurnal SSA modes of h and **middepth** SSC for the example data segment from the Dumbarton Bridge, 1993.

sent the **principal** spectral maxima of h (Figure 3) and contain 21.4 and 78.3% of the variance of h, respectively. The **RCs** of SSC are analyzed here instead of the raw time series because seasonal wind effects, the **subtidal** SSC variation caused by the spring-neap cycle, and tidal **harmonic** frequencies are absent from these **RCs**. The diurnal **RCs** of SSC for the Dumbarton Bridge example (**RC23** in Figure 4) and of h are shown in Figure 9. During spring tides (about days 9 and 21) the diurnal **RCs** of SSC and h are **180°** out of phase because diurnal ebb tides advect high SSC water to the Dumbarton Bridge from shallow water, and diurnal flood tides **advect** low SSC water landward to the bridge. During the neap tide (about day 15) the phase difference of the **RCs** varies because advective transport is relatively small. The phase difference of the semidiurnal **RCs** is similarly dependent on the **spring-neap** cycle, but only the diurnal **RCs** are shown for better visual clarity.

The diurnal and semidiurnal **RCs** for all the data segments indicate that tidal advection of SSC is significant during spring tides. For the diurnal **RCs** the lag from each SSC **RC** maximum to the preceding h **RC** maximum was determined and sorted by  $h_{rms}$  into four bins (Table 4). Spring tides are assumed to occur for  $h_{rms}$

Table 4. Mean and Standard Deviation of Lag of Diurnal **RC** Maxima of SSC from h as a Function of the Spring-Neap Cycle

Range of $h_{rms}$	Number of Maxima	Mean Lag, hours	Standard Deviation, hours
$h_{rms} < \overline{h_{rms}} - \sigma$ (neap tide)	82	11.1	4.9
$\overline{h_{rms}} - \sigma < h_{rms} < \overline{h_{rms}}$	241	11.1	4.8
$\overline{h_{rms}} < h_{rms} < \overline{h_{rms}} + \sigma$	166	12.5	3.9
$h_{rms} > \overline{h_{rms}} + \sigma$ (spring tide)	172	12.0	2.7

Mean  $h_{rms}$  ( $\overline{h_{rms}}$ ) is **75.51 cm**, and the standard deviation of  $h_{rms}$  ( $\sigma$ ) is **11.47 cm**.

greater than 1 standard deviation above the mean, and neap tides are assumed to occur for  $h_{rms}$  less than 1 standard deviation below the mean. For spring tides the mean lag is 12.0 hours, so SSC and  $h$  are nearly  $180^\circ$  out of phase, and the standard deviation is 2.7 hours. For neap tides the mean lag is slightly smaller, and the standard deviation is 4.9 hours. The standard deviation decreases as  $h_{rms}$  increases. The smaller standard deviation for spring tides indicates a more consistent phase relation between SSC and  $h$ . Results for the semidiurnal RCs are similar (Table 5). For spring tides the mean lag is 6.86 hours, and the standard deviation is 1.12 hours. For neap tides the mean lag is about the same, and the standard deviation is 2.18 hours.

Resuspension by large spring tidal currents also may contribute to the large SSC maxima, but local bottom shear stress and resuspension cannot account for the maxima. Two days of spring tide  $h$ , SSC, and  $u^2$  time series are shown in Figure 10. Two large maxima of  $u^2$ , one before and one after lower-low water, are not replicated in the SSC time series. SSC decreases during the second flood tide  $u^2$  maxima, so local resuspension and slow settling at slack water cannot explain the SSC maxima at low tide.

## Discussion

### Advective Transport

Advective transport is the dominant tidal process affecting SSC during spring tides. Water with higher SSC is advected to the channel sites from shallower water during spring ebb tides, and water with lower SSC seaward of the channel sites is observed during spring flood tides (Figures 7-9). During neap tides, advective transport is smaller, and these different water masses are not observed at the channel sites. This finding is similar to that of *Valle-Levinson* and *Wilson* [1994] for salinity in Long Island Sound, where a  $90^\circ$  phase difference between salinity and velocity indicated that advection was the dominant process affecting salinity during spring tides. Local resuspension by tidal currents also may affect SSC but cannot account for the observed SSC maxima (Figure 10).

One effect of advective transport is that SSC in the channel is well correlated with the seasonal variation in wind-shear stress (Table 2 and Figure 2). During spring and summer the increase in

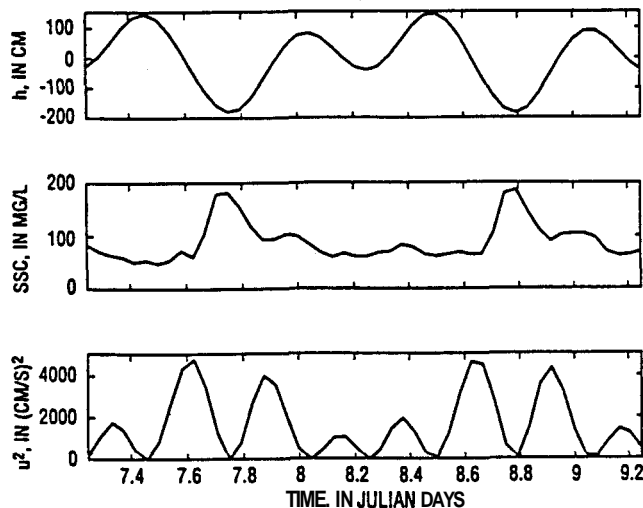


Figure 10. Example of SSC maxima at low spring tide and  $u^2$  for 2 days of a data segment from middepth at the Dumbarton Bridge, 1993. SSC is a measured value;  $h$  and  $u^2$  are calculated values.

the diurnal sea breeze in South Bay increases the mean wind stress, wind waves, and sediment resuspension in the relatively shallow water outside the main deep channel [*Lacy et al.*, 1996]. Tidal currents transport the resuspended sediments to the main channel, especially during spring tides.

### Spring-Neap Cycle

SSCs respond to the spring-neap cycle because of increased sediment resuspension during spring tides compared to neap tides, increased advective transport of water with higher SSC from shallow water during spring tides, and because relatively short periods of slack water limit the duration of deposition of suspended solids and consolidation of newly deposited bed sediment during the tidal cycle. As the tidal energy increases from a neap to a spring tide, water with higher SSC from shallower depths is advected to the channel; more bottom sediment is resuspended; and the quantity of easily erodible, unconsolidated sediment in the estuary increases. The duration of slack water, however, is only a few minutes (Figures 8 and 10), which does not permit deposition of the amount of suspended solids resuspended since the previous slack water. With each successive tidal cycle the minimum SSC increases (Figure 5). Thus suspended solids accumulate in the water column as a spring tide is approached. At spring tide, solids in suspension and in the bed are not in dynamic equilibrium as net resuspension during a tidal cycle continues and tidally averaged SSC increases. During the approximately 2 days after a spring tide the tidal energy decreases; the maximum SSC during a tidal cycle decreases as advective transport from shallow water decreases; the quantity of easily erodible, unconsolidated sediment in the estuary is greater than before the spring tide; the rate of net resuspension during a tidal cycle decreases to zero; and the minimum SSC reaches a maximum value. As the neap tide is approached, tidally averaged SSC decreases as the rate of net deposition increases to its maximum value, and advective transport of solids from shallow water decreases. Sediment accumulating on the bottom begins to consolidate, decreasing its erodibility [*Krone*, 1986]. At neap tide, suspended and bed solids are not in dynamic equilibrium as net deposition continues and tidally averaged SSC decreases. During the approximately 2 days after the neap tide the tidal energy increases, the rate of net deposition

Table 5. Mean and Standard Deviation of Lag of Semidiurnal RC Maxima of SSC from  $h$  as a Function of the Spring-Neap Cycle

Range of $h_{rms}$	Number of Maxima	Mean Lag, hours	Standard Deviation, hours
$h_{rms} < \overline{h_{rms}} - \sigma$ (neap tide)	176	6.94	2.18
$\overline{h_{rms}} - \sigma < h_{rms} < \overline{h_{rms}}$	470	6.69	2.18
$\overline{h_{rms}} < h_{rms} < \overline{h_{rms}} + \sigma$	338	6.77	1.78
$h_{rms} > \overline{h_{rms}} + \sigma$ (spring tide)	344	6.86	1.12

Mean  $h_{rms}$  ( $\overline{h_{rms}}$ ) is 75.51 cm, and the standard deviation of  $h_{rms}$  ( $\sigma$ ) is 11.47 cm.

decreases to zero, and tidally averaged SSC reaches a minimum value.

The relation between SSC and the spring-neap cycle in South Bay is similar but not identical to the relation observed in the Tamar Estuary by *Uncles et al.* [1994]. They observed that the relation between daily averaged SSC and tidal range in the Tamar Estuary was asymmetric with greater SSC when tidal range was decreasing (after a spring tide). *Uncles et al.* [1994] attributed this to the generation of a pool of easily erodible sediment by increasing spring tides that was available for resuspension by falling spring tides, similar to South Bay. A difference between the two estuaries is that the minimum SSC during the tidal cycle was constant in the Tamar Estuary [*Uncles et al.*, 1994, Figure 3] but varied with the spring-neap cycle in South Bay. The duration of high slack water in the Tamar Estuary is about 3 hours [*Uncles et al.*, 1994, Figure 4], during which time sediments resuspended during the preceding tidal phase deposit. The duration of slack water in South Bay is only a few minutes, which is insufficient for complete deposition of sediments resuspended during the preceding tidal phase when tidal energy is increasing.

The variance represented by RC1 and the correlation between lagged RC1 and  $h_{\text{min}}$  decrease landward from the San Mateo Bridge to channel marker 17 (Table 3). The variance in RC1 decreases in the landward direction because higher-frequency variations in SSC become more important relative to subtidal variations caused by the spring-neap cycle. The landward decrease in correlation indicates that subtidal variations in SSC up estuary are controlled less by the spring-neap cycle and more by other processes, such as wind wave resuspension and local runoff. The relatively small lag time at channel marker 17 (25.8 hours) is probably caused by more rapid settling. SSC is greatest at channel marker 17 (Table 1) because it is the closest site to shallow water where wind wave resuspension occurs and SSC is greatest. The suspended solids are cohesive, so settling velocity increases as SSC increases [*Krone*, 1962; *Mehta*, 1989; *Krask and Milligan*, 1992]. Greater settling velocity decreases the lag of RC1 behind the spring-neap cycle.

#### Tidally Averaged Transport of Suspended Solids

The seasonal variability in tidally averaged transport of suspended solids in South Bay can be inferred from the findings of this and other studies. When the spring and summer diurnal sea breeze is present, the wind-driven circulation is landward in shallow water and seaward in the main channel; and tidally driven, residual circulation south of the San Mateo Bridge is extremely weak [*Cheng and Gartner*, 1985; *Walters et al.*, 1985]. Wind waves generate higher SSC in shallower water, and the tidally averaged transport of these resuspended solids is landward in shallow water [*Lacy et al.*, 1996]. During spring tides, however, tidal advection is large enough to transport high SSC water from shallow water to the main channel (Figures 7-9). Some of these suspended solids become trapped in the main channel because of settling and limited tidal excursions. Once trapped in the main channel, suspended solids move seaward with the wind-driven circulation, creating a net seaward flux of suspended solids from the South Bay study area.

During autumn and winter, winds are smaller [*Gilliam*, 1962], and therefore wind waves and wind-driven circulation are smaller [*Lacy et al.*, 1996]. During winter and spring the density difference between South and Central Bays varies in response to freshwater discharge from the Delta and the return of oceanic water through the Golden Gate [*Walters et al.*, 1985]. Baroclinic circu-

lation can be either landward or seaward near the bottom of the main channel in South Bay where SSC is greatest. Plumes of high SSC water from the Delta have been observed in South Bay only north of the San Mateo Bridge [*Carlson and McCulloch*, 1974; *Powell et al.*, 1989] and are not a likely source of suspended solids in the study area. The variability or lack of baroclinic circulation; lack of wind and tidally driven, residual circulation in the study area; and smaller SSC caused by the absence of southerly wind shear (Figure 2) indicate that there is probably little import or export of suspended solids from the study area during autumn and winter.

The hypothesis that suspended solids are exported from the South Bay study area during summer and that net transport is negligible during winter is consistent with the seasonal change in the size distribution of bottom sediments and with calculations of sediment accumulation rates in South Bay. The amount of fine material in the bottom sediments of South Bay where the depth is less than 5 m is smallest during summer when wind waves suspend the finer material and make it available for transport [*Thompson et al.*, 1981; *Nichols and Thompson*, 1985]. Comparison of historical bathymetric surveys indicates that South Bay has a negative rate of sediment accumulation [*Conomos and Peterson*, 1977; *Krone*, 1979].

#### Conclusions

High-frequency SSC variations in South Bay are tidally driven, and nonlinear physical processes are significant. Tidal advection is most significant during spring tides when the tidal excursion is sufficiently large to transport high SSC water to the main channel from shallow water. During neap tides advection is less significant, and the tidal excursion is not large enough to transport high SSC water to the main channel from shallow water. SSC in the channel is well correlated with the seasonal variation in wind-shear stress due to advective transport of resuspended sediments from shallow water. Advective transport has a greater influence on SSC than local resuspension in the channel.

The findings of this and other studies indicate that the tidally averaged transport of suspended solids responds to seasonal variations of wind shear in South Bay. During summer the diurnal sea breeze generates wind waves that increase SSC and establish a landward flux of suspended solids in shallow water and a seaward flux of suspended solids in the main channel. Suspended solids in shallow water are transported to the main channel, primarily during spring tides when tidal excursions are greatest. Settling traps some suspended solids in the main channel, so there is a net export of sediment from South Bay during the summer. During winter, winds and SSC are smaller, and the wind-driven and baroclinic circulation are variable, so there is less tidally averaged transport of suspended solids.

The spring-neap cycle accounts for one half of the observed variance of SSC. Relatively short duration of slack water limits the duration of deposition of suspended solids and consolidation of newly deposited bed sediment during the tidal cycle, so as a spring tide is approached and at spring tide, suspended solids accumulate in the water column. As neap tide is approached and at neap tide, there is net deposition of suspended solids. SSC lags the spring-neap cycle by about 2 days. Perturbations in SSC caused by wind and local runoff from winter storms during the study period were usually much smaller than SSC variations caused by the spring-neap cycle.

Although the hydrodynamics of South San Francisco Bay are primarily tidally driven, SSC is most responsive to subtidal and

seasonal forcing mechanisms. A numerical or electronic filter provides an analogy for the response of SSC to the forcing factors. The energy of the input signal to the filter is mostly tidal energy at diurnal and semidiurnal frequencies. The filter damps high frequencies and amplifies lower frequencies. Thus most of the energy of the output signal of the filter (SSC) is at lower frequencies. In addition, the filter provides a 2-day phase shift at the fortnightly spring-neap frequency. The relatively slow deposition of suspended material and consolidation of newly deposited bed sediment compared to the duration of slack water are the mechanisms by which this filtering is achieved.

Acknowledgments. This study was done in cooperation with the California Regional Water Quality Control Board, San Francisco Bay Region, as part of the Bay Protection and Toxic Cleanup Program. The author would like to thank Ralph Cheng, Jim Cloern, Mike Dettinger, Ray Krone, and the anonymous reviewers for their helpful comments

## References

- Atwater, B. F., S. G. Conard, J. N. Dowden, C. W. Hedel, R. L. Macdonald, and W. Savage, History, landforms, and vegetation of the estuary's tidal marshes, in *San Francisco Bay: The Urbanized Estuary*, edited by T. J. Conomos, pp. 347-385, Pac. Div. Am. Assoc. for the Adv. of Sci., San Francisco, Calif., 1979.
- Buchanan, P. A. and D. H. Schoellhamer, Summary of suspended-solids concentration data Central and South San Francisco Bays, California, water years 1992 and 1993. *U.S. Geol. Surv. Open File Rep. 94-543*, 15 pp., 1995.
- Buchanan, P. A., D. H. Schoellhamer, and R. C. Sheplaine, Summary of suspended-solids concentration data. San Francisco Bay, California water year 1994, *U.S. Geol. Surv. Open File Rep. 95-776*, 56 pp., 1996.
- Carlson, P. R. and D. S. McCulloch, Aerial observations of suspended-sediment plumes in San Francisco Bay and the adjacent Pacific Ocean, *J. Res. U.S. Geol. Surv.*, 2(5), 519-526, 1974.
- Cheng, R. T. and J. W. Gartner, Tides, tidal and residual currents in San Francisco Bay, California--Results of measurements, 1979-1980, *U.S. Geol. Surv. Water Resour. Invest. Rep. 84-4339*, 1984.
- Cheng, R. T., and J. W. Gartner, Harmonic analysis of tides and tidal currents in South San Francisco Bay, California, *Estuarine Coastal Shelf Sci.* 21, 57-74, 1985.
- Cloern, J. E., Turbidity as a control on phytoplankton biomass and productivity in estuaries, *Cont. Shelf Res.*, 7(11/12), 1367-1381, 1987.
- Conomos, T. J., and D. H. Peterson, Suspended-particulate transport and circulation in San Francisco Bay, an overview, in *Estuarine Processes*, vol. 2, pp. 82-97, Academic, San Francisco, Calif., 1977.
- Dettinger, M. D., M. Ghil, C. M. Strong, W. Weibel, and P. Yiou, Software expedites singular-spectrum analysis of noisy time series, *Eos Trans. AGU*, 76(2), pp. 12, 14, and 21, 1995.
- Downing, J. P., R. W. Sternberg, and C. R. B. Lister, New instrumentation for the investigation of sediment suspension processes in the shallow marine environment *Mar: Geol.* 42, 19-34, 1981.
- Fishman, M. J. and L. C. Friedman, Methods for determination of inorganic substances in water and fluvial sediments, in *U.S. Geol. Surv. Techniques of Water Resources Investigations*, Book 5, Chap. A1, pp. 443, 1989.
- Flegal, A. R., G. J. Smith, G. A. Gill, S. Sanudo-Wilhelmy, and L. C. D. Anderson, Dissolved trace element cycles in the San Francisco Bay Estuary, *Mar: Chem.* 36, 329-363, 1991.
- Folger, D. W. Characteristics of estuarine sediments of the United States, *U.S. Geol. Surv. Prof. Pap.* 742.94 pp., 1972.
- Garratt, J. R. Review of drag coefficients over oceans and continents, *Mon. Weather Rev.*, 105(7), 915-929, 1977.
- Gilliam, H. *Weather of the San Francisco Bay Region*. 72 pp., Univ. of Calif. Press, Berkeley, 1962.
- Hammond, D. E., C. Fuller, D. Harmon, B. Hartman, M. Korosec, L. G. Miller, R. Rea, S. Warren, W. Berelson, and S.W. Hager, Benthic fluxes in San Francisco Bay, *Hydrobiologia*, 129, 69-90, 1985.
- Krank, K., and T. G. Milligan, Characteristics of suspended particles at an 11-hour anchor station in San Francisco Bay, California, *J. Geophys. Res.*, 97(C7), 11,373-11,382, 1992.
- Krone, R. B., Flume studies of the transport of sediment in estuarial shoaling processes, final report, Hydraul. Eng. Lab. and Sanit. Eng. Lab., Univ. of Calif., Berkeley, 1962.
- Krone, R. B., Sedimentation in the San Francisco Bay System in *San Francisco Bay: The Urbanized Estuary*, edited by T. J. Conomos, pp. 85-96, Pac. Div. Am. Assoc. for the Adv. of Sci., San Francisco, Calif., 1979.
- Krone, R. B., The significance of aggregate properties to transport processes, in *Estuarine Cohesive Sediment Dynamics. Coastal Estuarine Stud. Ser.*, vol. 14, edited by A. J. Mehta, pp. 66-84, Springer-Verlag, New York, 1986.
- Kuwabara, J. S., C. C. Y. Chang, J. E. Cloern, T. L. Fries, J. A. Davis, and S. N. Luoma, Trace metal associations in the water column of South San Francisco Bay, California, *Estuarine Coastal Shelf Sci.*, 28, 307-325, 1989.
- Lacy, J. R., D. H. Schoellhamer, and J. R. Burau, Suspended-solids flux at a shallow-water site in South San Francisco Bay, California, in *Proceedings of the North American Water and Environment Congress*, Am. Soc. Civil Eng., New York, 1996.
- Luoma, S. N., D. Cain, and C. Johansson, Temporal fluctuations of silver, copper, and zinc in the bivalve *Macoma balthica* at five stations in South San Francisco Bay, *Hydrobiologia*, 129, 109-120, 1985.
- Mehta, A. J., On estuarine cohesive sediment suspension behavior, *J. Geophys. Res.*, 94(C10), 14,303-14,314, 1989.
- Nichols, F. H. and J. K. Thompson, Time scales of change in the San Francisco Bay benthos, *Hydrobiologia*, 192, 121-138, 1985.
- Palmer, J. R., M. F. Friebel, L. F. Trujillo, and K. L. Markham, Water resources data, California, water year 1993, vol. 2, Pacific slope basins from Arroyo Grande to Oregon state line except Central Valley, *U.S. Geol. Surv. Water Data Rep.* CA-93-2.412 pp., 1994.
- Porterfield, G., Sediment transport of streams tributary to San Francisco, San Pablo, and Suisun Bays, California, 1909-1966, *U.S. Geol. Surv. Water Res. Invest.* 80-64, 91 pp., 1980.
- Powell, T. M., J. E. Qoern, and L. M. Huzzey, Spatial and temporal variability in South San Francisco Bay (U.S.A.), I. Horizontal distributions of salinity, suspended sediments, and phytoplankton biomass and productivity, *Estuarine Coastal Shelf Sci.*, 28, 583-597, 1989.
- Schoellhamer, D. H., Biological interference of optical backscatterance sensors in Tampa Bay, Florida, *Mar: Geol.* 110, 303-313, 1993.
- Thompson, J. K., F. H. Nichols, and S. M. Wienke, Distribution of benthic chlorophyll in San Francisco Bay, California, February 1980-February 1981, *U.S. Geol. Surv. Open File Rep. 81-1134*, 36 pp., 1981.
- Uncles, R. J., M. L. Barton, and J. A. Stephens, Seasonal variability of fine-sediment concentrations in the turbidity maximum region of the Tamar Estuary, *Estuarine Coastal Shelf Sci.*, 38, 19-39, 1994.
- Valle-Levinson, A. and R. E. Wilson, Effects of sill processes and tidal forcing on exchange in eastern Long Island Sound, *J. Geophys. Res.*, 99(C6), 12,667-12,681, 1994.
- Vautard, R., P. Yiou, and M. Ghil, Singular-spectrum analysis: A toolkit for short, noisy, chaotic signals, *Physica D*, 58, 95-126, 1992.
- Walters, R. A., R. T. Cheng, and T. J. Conomos, Time scales of circulation and mixing processes of San Francisco Bay waters, *Hydrobiologia*, 129, 13-36, 1985.

D. H. Schoellhamer, U.S. Geological Survey, 2800 Cottage Way, Room W-2233, Sacramento, CA 95825. (e-mail: dschoell@usgs.gov)

(Received May 4, 1995; revised December 12, 1995; accepted February 15, 1996.)